IEEE Access
Multidisciplinary | Rapid Review | Open Access Journal

Received January 30, 2021, accepted February 8, 2021, date of publication February 12, 2021, date of current version February 24, 2021.

Digital Object Identifier 10.1109/ACCESS.2021.3059115

Geometric-Pixel Guided Single-Pass Convolution Neural Network With Graph Cut for Image Dehazing

FAYADH S. ALENEZI[1], (Member, IEEE), AND SUBRAMANIAM GANESAN[2], (Life Senior Member, IEEE)
[1]Department of Electrical Engineering, College of Engineering, Jouf University, Sakaka 72388, Saudi Arabia
[2]Department of Computer Engineering, Oakland University, Rochester, MI 48309, USA
Corresponding author: Fayadh S. Alenezi (fshenezi@ju.edu.sa)

ABSTRACT One of the major shortcomings of existing image dehazing algorithms is in estimating scene transmittance, which has assumed many items in the existing algorithms. One key assumption has been pixel uniformity and smoothness. In this paper, we propose to solve the dehazing problem using a combination of single-pass CNN with graph cut algorithms. It considers the transmittance based on differential pixel-based variance, local and global patches and energy functions to improve the transmission map. The proposed algorithm was tested on different images and evaluated based on various evaluation metrics. Our results show more details when compared to four existing benchmark enhancement methods. The proposed method has one major drawback: the over-bright areas tend to lose some features in the final image.

INDEX TERMS Image enhancement, human visual perception, single pass-convolution neural network, graph cut.

I. INTRODUCTION

Accurate acquisition of natural images is important when visually inspecting the natural environment for proper use [1]. However, during severe weather conditions, atmospheric phenomena like haze or fog often scatter light and degrade the visual quality of natural images [2]. Haze or fog in natural images attenuates reflected light from the scene and creates a mixture of light and particles. This causes the image captured by the camera as hazy. Hazy images suffer from poor information quality, fainted surfaces, and color shift [3]. This hazy image is not suitable for various applications. Haze removal or defogging defined as a technique to reduce or remove interference due to haze. Defogging increases image information and is highly desired in computer vision and imaging applications [4].

Existing haze removal strategies are based on image enhancement, and image restoration [4]. Image enhancement methods focus on improving the image quality without considering the physical model of the imaging principle [5]. Such methods include histogram equalization [6], retinex theory [7], and saliency extraction [8]. These methods fail to recognize the reason and process of dehazing and, as such, lead to a more degraded image. The further degradation of the hazy image by image enhancement methods result from incomplete recovery effects or color distortion [1]. Image restoration methods focus on image recovery based on a physical model comprising atmospheric scattering [5], [9], [10]. These image recovery methods rely on auxiliary or prior information about the image [5]. The complexity of image recovery based on prior information makes this method not preferable by many researchers [5]. Haze removal methods (called supplementary) that combine traditional techniques with other image enhancement levels, such as histogram homogenization and wavelet analysis, have also been reported [4].

The existing and supplementary haze removal methods have shortcomings that have prompted further development of other techniques. For instance, Tan's [10] proposed haze removal techniques that yield final images with exaggerated contrast. Fattal's [11] proposed technique assumes no statistical relationship between the surface model and transmission and yields a resultant image with poor information, which results from poor color and brightness enhancement. Vazquez-Corral *et al.* proposed a method for color dehazing based on visual perception [2]. The visual inspection

The associate editor coordinating the review of this manuscript and approving it for publication was Shuping He.

This work is licensed under a Creative Commons Attribution-NonCommercial-NoDerivatives 4.0 License.
For more information, see https://creativecommons.org/licenses/by-nc-nd/4.0/

of the results shows a washout effect on darker regions because the method failed to consider the images' atmospheric light. Dai *et al.* developed techniques to distinguish between the sky and non-sky regions in a hazy image and then used improved restoration models based on dark channel prior to dehaze the images [4]. Dai *et al.*'s improved models were based on a physical model of sky scattering, poor adaptability of images with sky regions, and reduce the dark regions of the haze-free images [4]. Although Dai *et al.* generated haze-free images with better edges and good robustness to bright sky regions, the sky region results still produced darker and hazed background results just like those from Vazquez-Corral *et al.*'s method [2], [4]. He *et al.'s* contribution in dark channel prior reduction is widely used by many authors [12]–[15]. However, the soft matting employed in He *et al.'s* proposed algorithm make it computationally long [13]. He *et al.* made further improvements to their first technique by using a guided filter in place of soft matting to reduce computation and implementation costs [13]. He *et al.*'s technique was computationally complex and yielded results with poor edges and selective dehazing; that is, the technique only functioned well in non-sky area images [12]. Yang *et al.* introduced wavelet transforms in their proposed technique since haze only affects the low-frequency component of the image [16]. The proposed results from Yang *et al.* were darker since the method failed to notice the differential light from the scene and atmospheric light [16]. A combination of Artificial Neural Networks (ANN) and traditional dehazing methods exist and have shown promising results. The multilayer perceptron (MLP) has gained usage in many areas in image processing applications, such as in denoising and skin divisions [17]. Obulesu *et al.* proposed a technique that has exploited the MLP to yield the transmission map of the hazy image directly from the dark channel to help stretch contrast and amplify the dynamic range of the restored image [17]. Visual inspection of Obulesu *et al.*'s proposed results shows the restored image retains haze in some parts of the image, especially towards the horizon, resulting in poor edges [17].

The existing single image dehazing techniques are based on many assumptions, which lead to inaccuracies in the final image. Promising state-of-the-art methods such as that of [18] are based on a geometric boundary constraint, but they still rely on some assumptions, leading to inaccuracies in the results. The proposed paper explores using the geometric-variance pixel-based guided local and global relationships to estimate the transmittance medium to extract a haze-free image accurately. This is achieved via estimation of transmittance medium through local and global pixel variance within image neighborhood. The proposed extensions of high-low pixel gradient variance-based boundary in the global and local Markov fields in the energy function smoothen and constraint the connection between local and global pixel neighborhoods. These two critical geometric-based proposal helps improve dehazed image features. The rest of the paper covers background information followed by a description of the proposed method and, finally, an illustration of the proposed method's performance.

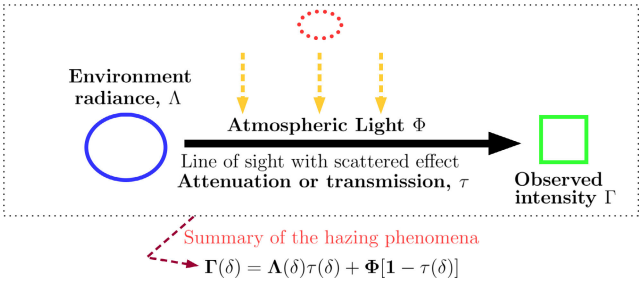

FIGURE 1. A visual representation of formation of scattering effect.

II. CONTRIBUTION

The paper has three significant contributions: a novel combination of single-pass CNN with graph cut algorithms to yield novel dehazed image; transmittance medium based on a variance of pixels based on the local and global based neighborhood (serves to enhance local and global image features); local and global pixel-based energy function based on pixel variance constraints of respective neighborhoods to improve transmission map (serves to increase finer details of the dehazed image).

III. MATERIALS AND METHODS

A. MATERIALS

1) ATMOSPHERIC SCATTERING MODEL

The hazy conditions, formulated in Fig. 1, occur when there are many particles suspended in the environment, causing a scattering effect on the light [1], [4]. Scattered particles during hazy weather conditions enable the attenuation of reflected light on the surfaces of objects. The attenuated light weakens the brightness of the image and reduces the image's resolution as the forward scattering effect infinitely continues between the surfaces and particles [1]. The backscattering of atmospheric particles on natural light leads to image contrast reduction, hue deviation, and image saturation [19]. These back and forward scattering effects on sensor light and natural light in hazy images are widely modeled through a dark channel prior model as follows [1], [3]–[5]:

$$\Gamma(\delta) = \Lambda(\delta)\tau(\delta) + \Phi\left(1 - \tau(\delta)\right). \tag{1}$$

In (1), $\Gamma(\delta)$ is the observed image or brightness of the haze image as received by the observer at pixel δ, $\Lambda(\delta)$ is the scene or environment radiance of the haze-free image; Φ is the atmospheric light, and $\tau(\delta)$ is the attenuation or transmittance medium, which ranges between 0 and 1, and thus can be redefined as,

$$\left(\tau(\delta) = e^{-\eta\xi(\delta)}|_{\tau(\delta)\in[0,1]}\right), \tag{2}$$

where η is the scattering coefficient of the atmosphere, and $\xi(\delta)$ is the depth of the scene. Equation (2) is applicable when the atmosphere is homogeneous, otherwise, $\tau(\delta)$ is given by (3).

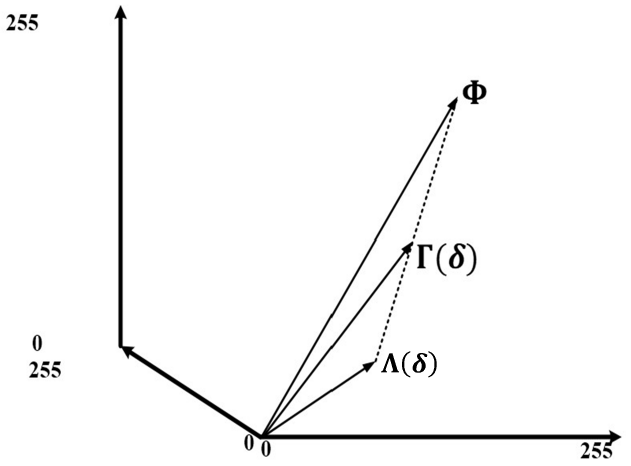

FIGURE 2. A visual representation of neighborhood pixel correlation within a region for first image example.

FIGURE 3. Smallest region of the dehazed image.

Fig. 2 shows the essence of haze removal from an image restoration perspective. This means that from the observed image brightness, $\Gamma(\delta)$, we remove atmospheric light, Φ, while compensating for attenuation of the light, $\tau(\delta)$, to restore clear scenes, $\Lambda(\delta)$. The Fig. 2 suggests RGB color space vectors $\Lambda(\delta)$, Φ and $\Gamma(\delta)$ in (2) are coplanar from a geometric point of view. Fig. 2 also shows that the end points of vectors $\Lambda(\delta)$, Φ and $\Gamma(\delta)$ are collinear and transmission, $\tau(\delta)$, is the ratio of the length of the two lines, as defined in (3).

$$\tau(\delta) = \left\| \frac{\Phi - \Gamma(\delta)}{\Phi - \Lambda(\delta)} \right\| \tag{3}$$

Equation (2) is transformed to (4) to show that haze removal depends on an accurate retrieval of $\Lambda(\delta)$, Φ, and $\tau(\delta)$ from $\Gamma(\delta)$. $\Lambda(\delta)\tau(\delta)$ represents direct attenuation and shows emissivity decay the of natural environment in the medium. $\Phi(1-\tau(\delta))$ is air-light based on previously scattered light, which leads to a shift in natural environment color. Therefore, the longer the distance between the sensor and the object, the greater the attenuation ($\Lambda(\delta)\tau(\delta)$) and scattering effect ($\Phi(1 - \tau(\delta))$), which suggests that transmission is exponential, as shown in (2).

$$\Lambda(\delta) = \frac{\Gamma(\delta) - \Phi}{\tau(\delta)} + \Phi. \tag{4}$$

2) CONVOLUTION NEURAL NETWORK

The literature on the structure and architecture of Convolution Neural Network (CNNs/ConvNets) are presented in the following existing papers [20]–[27].

B. GEOMETRIC-PIXEL GUIDED SINGLE-PASS CONVOLUTION NEURAL NETWORK WITH GRAPH CUT FOR IMAGE DEHAZING

1) TRANSMISSION MAP

We first define the pixel value changes along the smallest regions of the hazed image (see Fig. 3) as Δp. The pixel changes also reflect changes in image features. If we denote the variance of these changes as $\zeta = (\Delta p)^2$, when $\zeta \to 0$, the change is invisible. Since pixel values are between 0 and 1, then variance in the neighboring pixels, q is given by $\|\Delta p - \Delta q\|^2$, $\|.\|$ is the magnitude of the pixels. We can therefore denote threshold process in input image I_d as

$$I_{threshold} = \frac{\|\Delta p - \Delta q\|^2}{p - q}. \tag{5}$$

Equation (5) is analogous to (3), that is,

$$I_{threshold} = \frac{\|\Delta p - \Delta q\|^2}{p - q} \simeq \left\| \frac{\Phi - \Gamma(\delta)}{\Phi - \Lambda(\delta)} \right\| = \tau(\delta) \tag{6}$$

Thus, the transmittance medium defined by (2) becomes

$$\frac{\|\Delta p - \Delta q\|^2}{p - q} \simeq \left(\tau(\delta) = e^{-\eta\xi(\delta)}|_{\tau(\delta)\in[0,1]} \right). \tag{7}$$

We replace the results from (7) into (1) to obtain

$$\Gamma(\delta) = \Lambda(\delta)\left(\frac{\|\Delta p - \Delta q\|^2}{p - q} \right) + \Phi\left(1 - \left(\frac{\|\Delta p - \Delta q\|^2}{p - q} \right) \right). \tag{8}$$

Equation (8) indicates that one of the main problems of image dehazing is solved since, unlike in the beginning, when three unknowns were present, only two unknowns are left, that is, Φ and $\Gamma(\delta)$. However, Φ can be estimated based on Retinex theory [7] atmospheric light brightest pixel from $\Phi = [max(R), max(G), max(B)]^t$, where R,G,B are the three color channels in the image and t determines the weights of the colors.

2) GLOBAL AND LOCAL MARKOV RANDOM FIELDS

The general energy functions of Markov random field (MRF) models for many existing states of the art dehazing models is [28]–[30], [30], [31]

$$E(x) = \sum_{m\in v} \phi_m(\chi_m) + \sum_{(m,n\in\epsilon)} \psi_{m,n}(\chi_m, \chi_n) \tag{9}$$

χ_m is the configuration of pixel m in the image, ϕ_m is unary potential and is the cost of the label assigned to pixel m. ϕ_m is computed using color, texture, location, and shape of the image. $\psi_{m,n}$ is pairwise terms, and is considered smooth terms and defined by edge features based on the difference between neighboring pixels. $\psi_{m,n}$ enables a smoothing of object boundaries in the haze-free image. Equation (9) allows the extraction of details from the haze-free image. However, the use of the energy function described by (9) is not common in image processing due to complications associated with algorithms for optimizing the cost functions. Although (9) is not common in image processing, its modification has found immense use.

Scene depth changes are usually gradual and vary from local to global neighborhood. Therefore, accurate estimation of depth variation would be on both the local and global image features. The existing state of the art dehazing models such as [28] designed local consistent MRF model extracting local pixel blocks. The haze-free images by [28] present color oversaturation in some regions. This was due to the consideration of only local pixels in the design of MRF. Qu *et al.* [28] proposed a higher-order method in MRF to solve the smoothing problem associated with statistics of the entire image. The higher-order terms were extended in MRF (9) as:

$$E(x) = \sum_{m \in v} \phi_m(\chi_m) + \sum_{(m,n \in \epsilon)} \psi_{m,n}(\chi_m, \chi_n) + \sum_{c \in S} \varphi_c(\chi_c) \tag{10}$$

where $E(x)$ is still the general term for energy functions of Markov random field (MRF) S is a set of image regions defined on super-pixels with higher-order pixels φ_c. Unlike the existing image dehazing models, which focus on the relationship between neighboring pixels and super-pixels with local image patches, we have defined the proposed method's global and local image blocks. In this model, the color feature is also a representative of both global and local color moment. This approach ensured atmospheric light used represents the relationship between global and local pixels and super-pixels.

To model the long and short-range interactions, that is, the global and local neighborhood pixels and super-pixels relationships, we consider the global relationship between neighboring local pixels as suggested by [32]. The MRF constructed has edge cost representing the neighboring pixel's consistency in overlapping regions. Suppose we denote volume of patches as m and pixel indices $\chi = \{\chi_i | i = 1, \ldots, n\}$ and the number of nodes n while the number of labels i^{th} node is k_i, thus the patches in the neighbourhood is denoted by m_i. Suppose the unary and pairwise potential and their ratio are $\phi_g(\chi_i)$, $\psi_g(\chi_i, \chi_{i'})$ and λ_g respectively with i' indicating index of neighbouring patch of m_i and g indicate global-level MRF. Supposed it assumed that the image is likely to have a high gradient boundary, the unary potential $\phi_g(\chi_i)$ is defined as

$$\phi_g(\chi_i = j) = log\left(\frac{1}{|c(\mathbf{X}_i^j)|} \sum_{m \in c(\mathbf{X}_i^j)} \left|\frac{\partial Im}{I_{max}}\right|\right) \tag{11}$$

where ∂Im denote the magnitude of intensity gradient of pixel m and I_{max} in the maximum intensity of the pixels in the haze image; thus, a patch with higher pixel gradient variance exhibit lower cost. The pairwise potential $\psi_g(\chi_i, \chi_i')$ defined by (12) is based on the assumption of the existence of smooth connection between local and global patches [32], [33].

$$\psi_g(\chi_i = j, \chi_{i'} = j') = -log\left(\frac{2\sum_{m \in \mathbf{m_i} \cap \mathbf{m_{i'}}} \mathbf{X_i^j}(m)\mathbf{X_{i'}^{j'}}(m)}{\sum_{m \in \mathbf{m_i} \cap \mathbf{m_{i'}}} \mathbf{X_i^j}(m) + \mathbf{X_{i'}^{j'}}(m)}\right) \tag{12}$$

where $\mathbf{m_i} \cap \mathbf{m_{i'}}$ represent overlapping pixels within local and global patches. Suppose the pairwise potential $\psi_g(\chi_i, \chi_i') = 0$. Then there is no difference between the pixel in the patches. This assumption can be misleading on weaker correlations, thus requiring more constrained terms to enhance smooth connection. Therefore, (11) is extended to incorporate variance high-low gradient variance boundary as

$$\phi_{gl}(\chi_i = j) = log\left(\frac{1}{|c(\mathbf{X}_i^j)|} \sum_{m \in c(\mathbf{X}_i^j)} \left|\frac{\partial Im}{(I_{max} - I_{min})^2}\right|\right), \tag{13}$$

and pairwise potential as

$$\psi_{gl}(\chi_i = j, \chi_{i'} = j') = -log\frac{M_{pp}}{M_{pd}} \tag{14}$$

where

$$M_{pp} = 2 \sum_{m \in \mathbf{m_i} \cap \mathbf{m_{i'}}} \mathbf{X_i^j}(m)\mathbf{X_{i'}^{j'}}(m),$$

$$M_{pd} = \sum_{m \in \mathbf{m_i} \cap \mathbf{m_{i'}}} \left[\left|\mathbf{X_i^j}(m) + \mathbf{X_{i'}^{j'}}(m)\right|^2 + \left|\mathbf{X_i^j}(m) - \mathbf{X_{i'}^{j'}}(m)\right|^2\right.$$

The energy function of the global-local consistency MRF proposed is thus represented as

$$E(x) = \sum_{m \in v} \phi_m(\chi_m) + \sum_{(m,n \in \epsilon)} \psi_{m,n}(\chi_m, \chi_n) + \sum_{c \in S} \varphi_c(\chi_c) + \sum_i \phi_{gl}(\chi_i) + \lambda_g \sum_{i,i'} \psi_{gl}(\chi_i, \chi_i'). \tag{15}$$

The graph cut is used to optimize the (15). The graph convolution neural network has found tremendous application in many image processing [34]–[43]. The extension of global and local consistency in (15) also serves to caution the proposed graph cut convolution neural network from the problem of smoother far apart pixels. Besides, it also serves to avoid over saturation of color and enhances sharper boundaries.

Graph cut has two main parts, data and regularization part [44]. The data part measures the image data conformity, such as image features. The regularization part smoothens the boundaries of the different conformity areas. The rest of literature and procedure for graph cut method has been extensively discussed by [44]–[49]. The effectiveness of the proposed method presented in a summary in Fig. 4 is presented in Fig. 9.

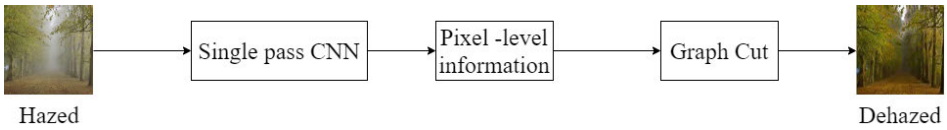

FIGURE 4. Schematic view of the proposed Geometric-Pixel Guided Single-Pass Convolution Neural Network with Graph Cut for Image Dehazing.

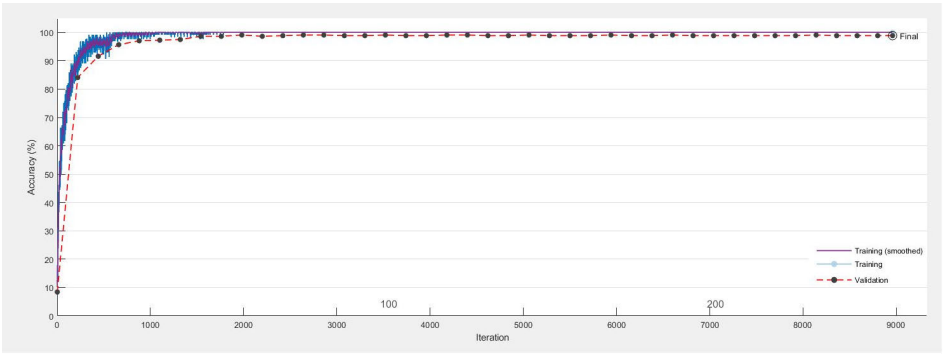

FIGURE 5. Example of one of the accuracy plots obtained during the training.

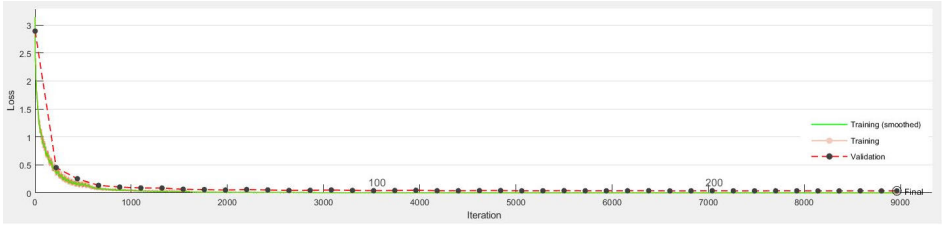

FIGURE 6. Example of one of the loss plots obtained during the training.

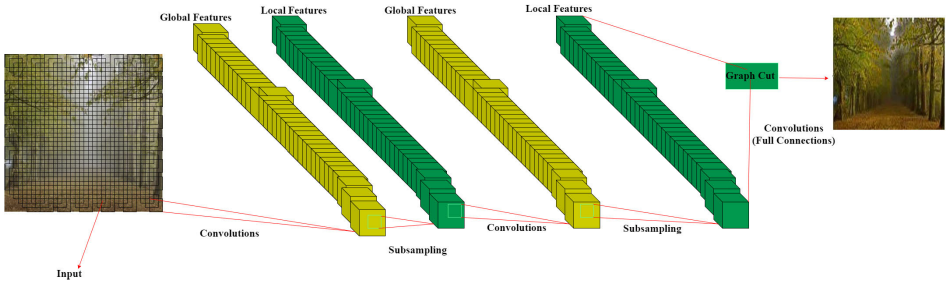

FIGURE 7. The schematic detail shows the proposed architecture with seven neurons in the second hidden layer, eight neurons in the third hidden layer, and a single output. The series contains alternating global and local feature extraction before full connection then graph cut to obtain the final dehazed image.

IV. EXPERIMENTS

A. DATA AND IMPLEMENTATION

The proposed method (summarized in Fig. 7 and detailed in Fig. 8) has been applied to various images (presented in Figs. 11-13) sourced from different database. These images were resized to a size of (28,28) to keep computational complexity low. The images presented in Fig 11-13 are examples chosen from a dataset of 24 examples used during the experiment. However, the quality metrics presented in Table 2 are based on the results of the 24 images used during the experiment, whose parameter values are summarized in Table 1. A total of 10560 images were used to train the network, from the 440 partitions from 24 images samples. 1320 images used for validation from the simulated clear images for the images presented in Fig. 13. The images whose results are presented in Figs. 11 and 12, validation images were extracted from the regions with rich textures. Thus, for these set of results, the quality could be compromised due to the lack of ground truth to validate the images. The final images output were reconstructed from 440 to yield results

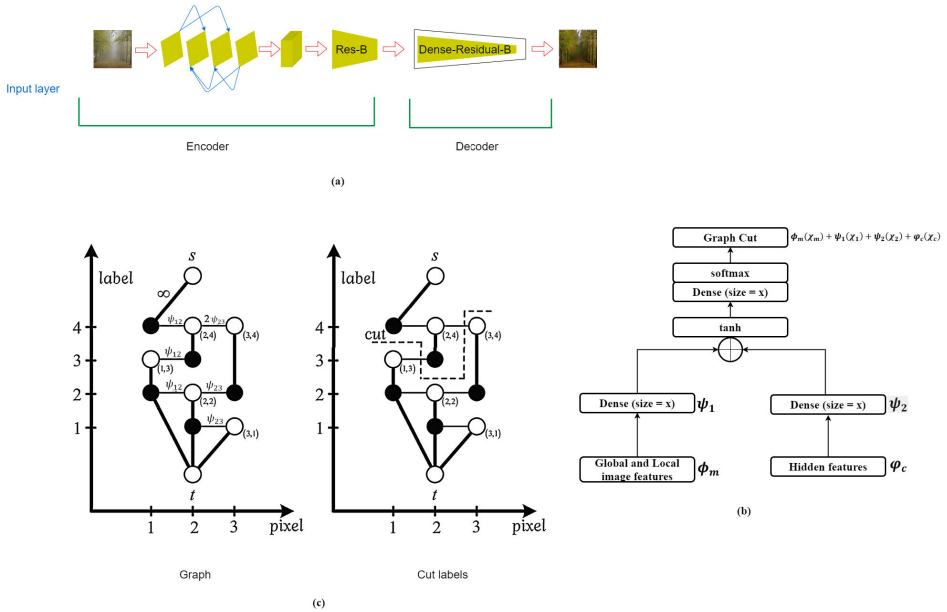

FIGURE 8. Detailed CNN for the proposed dehazing method with the encoder and decoder are similar except for the residual phase. The residual function ensures that each hidden neuron is fully connected, enhances the learning rate, and converges the training data set model. (b) The dense-residual phase is composed of softmax, which feeds information to the (c) graph-cut algorithm, which conforms image features and smoothens the boundaries of varying conformity areas.

FIGURE 9. Comparison of the effect of proposed energy function on the image features with the existing state of the art algorithm that tries to utilize the graph cut theory by [45]. It is visible how effective the proposed method has extracted extra features in the dehazed image compared with existing [45] results.

presented in Figs. 11-13. An example of accuracy and loss plots obtained during the training is also presented in Fig. 5 and Fig. 6 respectively. The partition helped organize images into patches of similar local and global neighbourhoods. The training processed for the proposed dehazing technique was performed on BIZON X5000 G2 with 16GB RAM.

Fig. 5 and 6 indicate accuracy and loss function across epoch for over the number of iteration. Both figures indicate a narrow gap between training and iteration, indicating less overfitting. Therefore, the model is assumed to give the desired results during training.

Figs. 8a consists of input, encoder and decoder. The encoder consists of convolution neural networks which extract global and local features from the hazy images. The decoder function like encoder except for its residual function which contain graph cut (see Figs. 8b - 8c). The residual decoder function allows full connection with other neurons, thus enhancing the learning rate and converging the training

FIGURE 10. Comparison showing the first image dehaze-cut results and second image the proposed results. The red and green patches shows the effectiveness of the proposed method in comparison with the existing dehaze-cut method [45]. The red and green patches indicate the effectiveness of that the proposed results is more blurry but on closer view has more details than the existing dehaze cut.

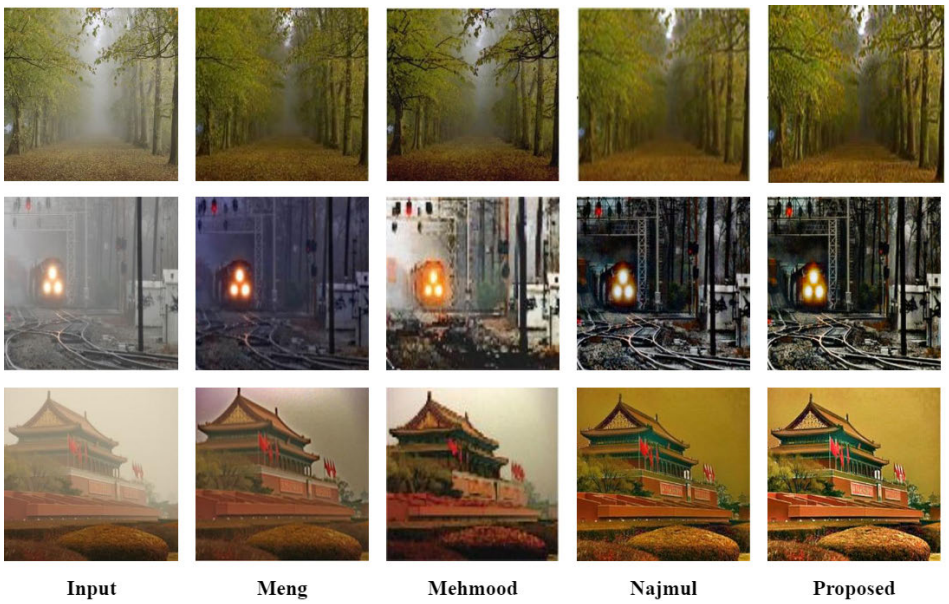

FIGURE 11. Summary of the test comparison showing the original image in the first column followed by the results from [18], [52], [54] and the results from the proposed algorithm in the last column.

TABLE 1. Values obtained and used during the experiment for the proposed dehazing algorithm.

Item	Experimental Value Range
Accuracy	$97.06\% - 98.72\%$
Training Time	$(19\text{min}38\text{sec}) - (20\text{min}53\text{sec})$
Learning Rate	$0.095 - 0.015$
Validation Frequency	$150 - 320$
Iterations	$10500 - 16720$
Epoch	$240 - 320$
Estimated Momentum	$0.85 - 0.92$ [50]
Estimated λ_g	98 [50]

model. Figs. 8c is build graph designed to minimize energy problem presented in (15). The graph consists of nodes corresponding to image pixels and pixel labels. The pixels are weighted based on its label. The cut consists of a configuration of pixels at its maximum label. The cut ensures the energy is minimal at all configurations.

B. EVALUATION METRICS

The proposed method's performance evaluation is conducted using five image quality criteria, including: (i). Entropy [51]; (ii). e (visible edges) [52]; (iii). r (edge preservation performance) [52]; (iv). Contrast and (v) Homogeneity [53]. These criteria are chosen based on the proposed method's objective: improving information content, measuring human visual quality and textural features, and similarities of a dehazed image.

TABLE 2. Comparison of mean and standard deviation of performance evaluation metrics of the proposed and existing state of the art algorithm for example presented in Fig. 11. *e* and *r* are blind assessment indicators. *e* assess increased rate of visible edges while *r* assess edge preservation performance. Higher values of μ indicate better method while lower values of σ show consistency of the results.

Example	Algorithm	μ and σ	Entropy	e	r	Contrast	Homogeneity
Fig. 11	Meng [18]	μ	6.9660	20.50	1.83	0.33	0.90
		σ	$\pm$0.54	$\pm$2.93	$\pm$0.35	$\pm$0.11	$\pm$0.03
	Mehmood [52]	μ	7.62	21.12	1.93	0.72	0.83
		σ	$\pm$0.28	$\pm$2.68	$\pm$0.07	$\pm$0.35	$\pm$0.09
	Najmul [54]	μ	7.27	21.50	3.29	0.77	0.83
		σ	$\pm$0.09	$\pm$4.49	$\pm$0.06	$\pm$0.43	$\pm$0.06
	Proposed	μ	7.64	22.40	3.40	1.22	0.82
		σ	$\pm$0.03	$\pm$2.44	$\pm$0.02	$\pm$0.05	$\pm$0.02
Fig. 12	Meng [18]	μ	7.32	13.60	1.76	0.55	0.84
		σ	$\pm$0.44	$\pm$1.81	$\pm$0.32	$\pm$0.16	$\pm$0.03
	Najmul [54]	μ	7.24	22.65	2.88	1.32	0.75
		σ	$\pm$0.37	$\pm$3.98	$\pm$0.19	$\pm$0.90	$\pm$0.08
	Proposed	μ	7.53	21.09	3.15	1.91	0.85
		σ	$\pm$0.23	$\pm$2.45	$\pm$0.32	$\pm$1.14	$\pm$0.01
Fig. 13	Meng [18]	μ	6.29	19.49	1.81	0.89	0.72
		σ	$\pm$0.16	$\pm$2.09	$\pm$0.58	$\pm$0.94	$\pm$0.07
	Najmul [54]	μ	6.26	23.71	2.14	1.91	0.69
		σ	$\pm$0.25	$\pm$2.05	$\pm$0.07	$\pm$0.56	$\pm$0.06
	Proposed	μ	6.32	16.12	4.51	1.95	0.77
		σ	$\pm$0.13	$\pm$1.98	$\pm$0.31	$\pm$0.49	$\pm$0.05

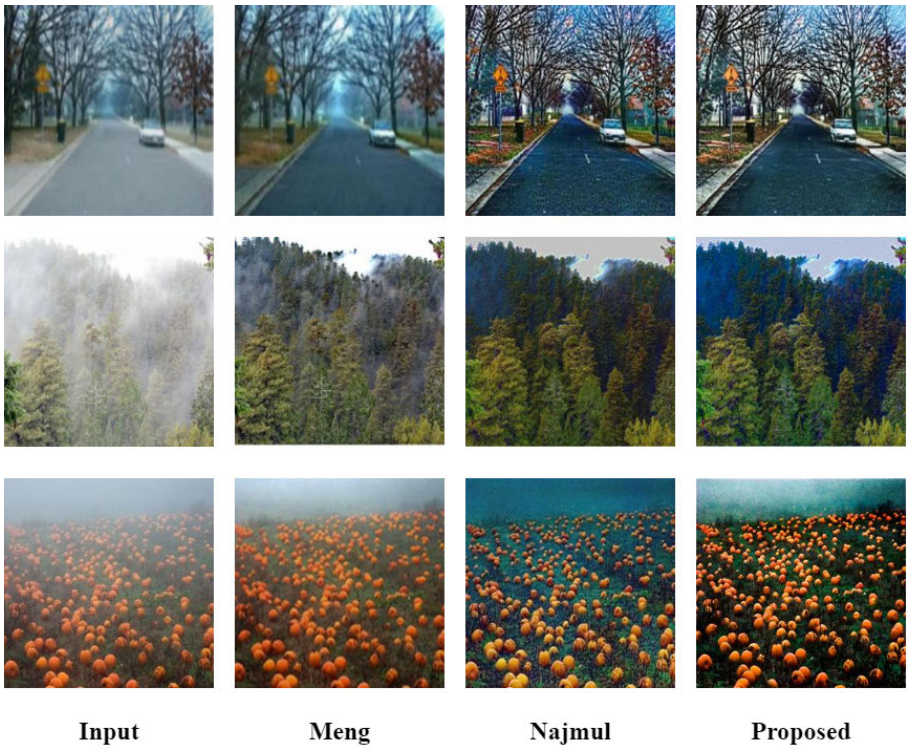

FIGURE 12. Summary of the test comparison showing the original image in the first column followed by the results from [18], [54] and the results from the proposed algorithm in the last column.

C. RESULTS ANALYSIS AND COMPARISON

1) QUANTITATIVE COMPARISON

2) COMPARISON ANALYSIS

In all the cases, (see Table 2), the images resulting from applying the proposed algorithm have averagely higher entropy, e, r, contrast and homogeneity, SSIM, and WPSNR. This suggests the proposed method resulted in a dehazed image with improved information content, visibility, and better texture than existing methods (Fig. 4, 11-15). The difference in the textural properties of the proposed method is compared

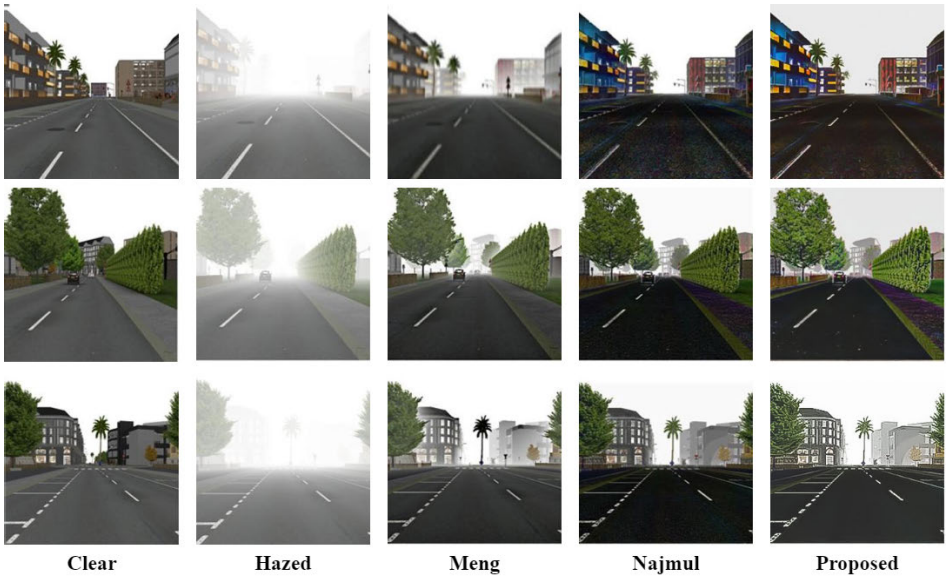

FIGURE 13. Summary of the test comparison showing the original image in the first column followed by the results from [18], [54] and the results from the proposed algorithm in the last column.

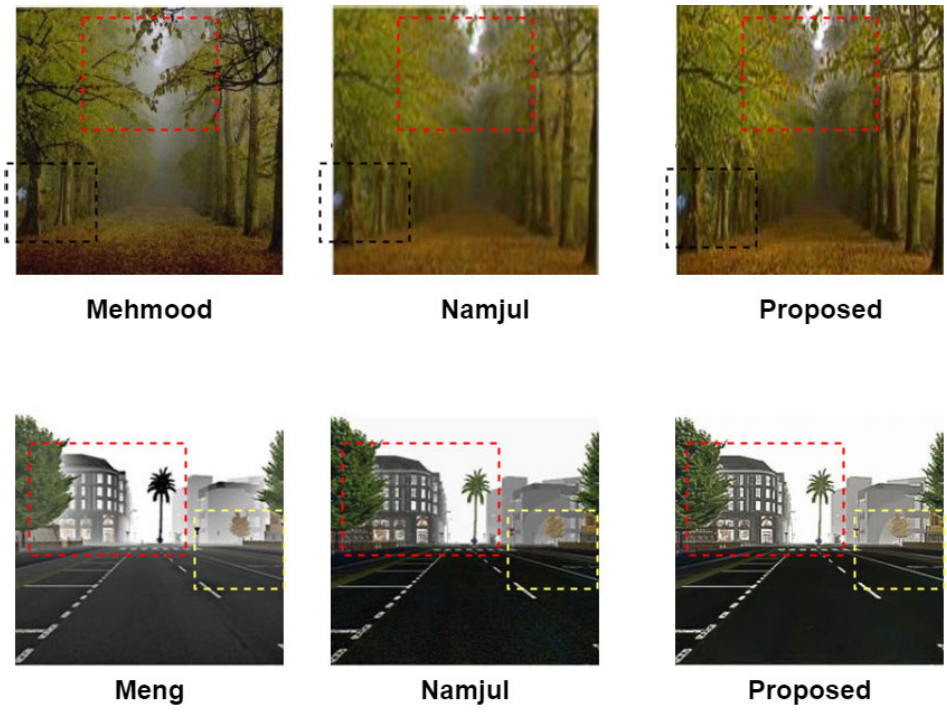

FIGURE 14. Summary of the test comparison showing the extracts of fundamental differences in the results of the proposed methods and the existing state of the art methods Meng [18], Najmul [54] and Mehmood [52]. The extract shows the proposed method gives images with better visibility and clarity of features.

with those of the state of the art method in Fig. 14-15. The difference in the textures Fig. 14-15 shows that a modification of the combination of graph cut and single-pass CNN with modified energy function and pixel-guided transmission ultimately yields a better dehaze image. A further visual inspection of patched sections of the proposed results in Fig. 14 compared to the existing methods reveals its strength and weakness.

The proposed method's major strength lies in its ability to extract finer details in the dehazed images (see red and black patches in Fig. 14). The red patched areas, for instance, in the regions marked red and black, tend to have more details

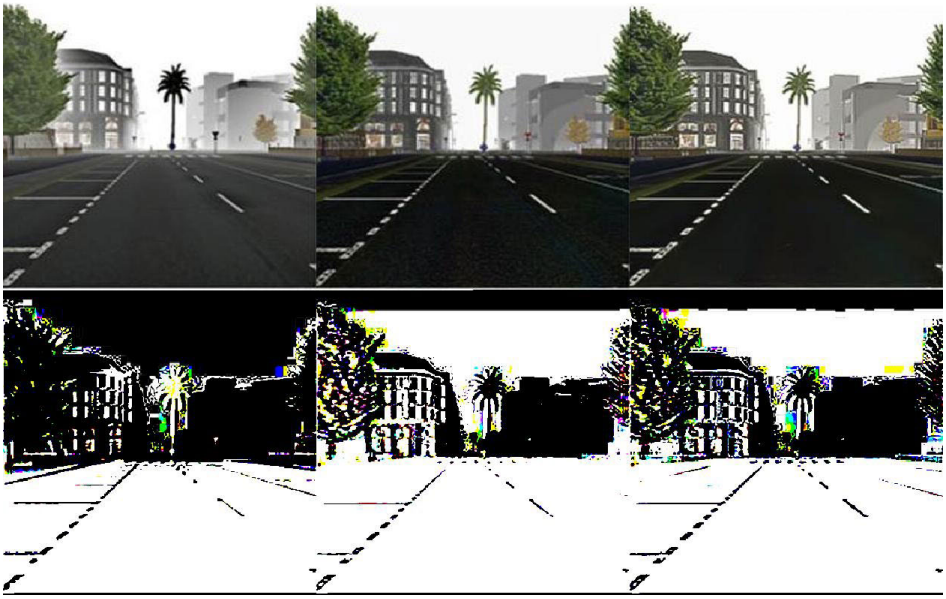

FIGURE 15. Comparison showing the extracts of features between the clear and dehazed image for the proposed methods and the existing state of the art methods, beginning with Meng [18], Najmul [54] and proposed. The extract in the last row shows the proposed method gives images with more features.

than those in Mehmood [52] and Najmul [54]. The extra information is attributed to the proposed pixel differential-based transmittance medium, which focuses on the global and local patches' pixel difference. This explains the addition of some tree leaves in the patched sections. The estimation of transmittance medium via local and global pixels with image neighborhood distinguishes regions, leading to more information extraction.

The visual inspection of patched sections of the proposed results in Fig. 14 compared to the existing methods reveals its weakness. While the proposed method focuses on extracting finer details of the dehazed images (see red and black patches), the regions with excess light tend to lose some information (see also Fig. 10). The red patched areas, for instance, in the areas marked red and black, tend to lose some information, specifically in the over bright regions compared to those in Mehmood [52] and Najmul [54]. This is attributed to the proposed pixel differential-based transmittance medium. The pixel difference of the global and local patches functions by treating pixels within regions with excess light. This explains the missing of some tree leaves in the patched sections. The estimation of transmittance medium via local and global pixels with image neighborhood makes some regions have similar traits. This also explains the sky and roof color similarity in Fig. 11-15 in all the examples.

In all the examples presented, extra features in the proposed image results compared to existing results from the proposed novel estimation of transmittance medium. The standard deviation values in all cases, as presented in Tables 2, show lower values than the corresponding benchmark algorithms. Table 2 also shows that our proposed algorithm has a lower entropy of 6.32 than Najemul's algorithm entropy of 6.25 Meng's algorithm entropy of 6.29. Also, our proposed algorithm has better consistency than others. These indicate that the proposed method gives more consistent and predictable results than existing algorithms.

V. CONCLUSION

This paper presents a novel geometric-pixel guided single-pass Convolution Neural Network with Graph Cut for Image Dehazing. We propose to solve the dehazing problem using a combination of single-pass CNN with graph cut algorithms. The method considers the transmittance based on differential pixel-based variance, local and global patches and energy functions to improve the transmission map. Through results presented and demonstrated in examples, the paper demonstrates that the proposed algorithm gives a better-dehazed image than those of the existing state of the art methods as shown in Fig. 10. Fig. 14 and Fig. 15, show that our proposed method gives images with better visibility, clarity of features and more features. In general, our results show more details when compared to four existing benchmark enhancement methods. The proposed method has a major weakness; that is, the over-bright areas tend to lose some final image features. The weakness is also its strength and arises due to the proposed novel estimation of the transmittance medium. Future research could consider a combination of our method with other existing algorithms such as dark channel prior, since at least one color channel of an rgb image has some pixels of the lowest intensities. Future research could also consider combining conditions for atmospheric homogeneity and ratio

between the segments during estimation of transmittance medium.

REFERENCES

[1] L. Peng and B. Li, "Single image dehazing based on improved dark channel prior and unsharp masking algorithm," in *Proc. Int. Conf. Intell. Comput.* Wuhan, China: Springer, 2018, pp. 347–358.

[2] J. Vazquez-Corral, A. Galdran, P. Cyriac, and M. Bertalmío, "A fast image dehazing method that does not introduce color artifacts," *J. Real-Time Image Process.*, vol. 17, no. 3, pp. 607–622, 2018.

[3] B. Li, W. Zhang, and M. Lu, "Multiple linear regression haze-removal model based on dark channel prior," in *Proc. Int. Conf. Comput. Sci. Comput. Intell. (CSCI)*, Dec. 2018, pp. 307–312.

[4] D. Zhen, H. A. Jalab, and L. Shirui, "Haze removal algorithm using improved restoration model based on dark channel prior," in *Proc. Int. Vis. Informat. Conf.* Kuala Lumpur, Malaysia: Springer, 2019, pp. 157–169.

[5] E. Alharbi, Y. Shan, P. Ge, and H. Wang, "An image dehazing method based on an improved retinex theory," in *Proc. Int. Conf. Comput. Eng., Inf. Sci. Appl. Technol. (ICCIA)*, 2016, pp. 108–114.

[6] J.-H. Kim, J.-Y. Sim, and C.-S. Kim, "Single image dehazing based on contrast enhancement," in *Proc. IEEE Int. Conf. Acoust., Speech Signal Process. (ICASSP)*, May 2011, pp. 1273–1276.

[7] E. H. Land, "The retinex theory of color vision," *Sci. Amer.*, vol. 237, no. 6, pp. 108–129, 1977.

[8] J. Zhao, Y. Chen, H. Feng, Z. Xu, and Q. Li, "Infrared image enhancement through saliency feature analysis based on multi-scale decomposition," *Infr. Phys. Technol.*, vol. 62, pp. 86–93, Jan. 2014.

[9] J. Liang, L. Ren, E. Qu, B. Hu, and Y. Wang, "Method for enhancing visibility of hazy images based on polarimetric imaging," *Photon. Res.*, vol. 2, no. 1, pp. 38–44, 2014.

[10] R. T. Tan, "Visibility in bad weather from a single image," in *Proc. IEEE Conf. Comput. Vis. Pattern Recognit.*, Jun. 2008, pp. 1–8.

[11] R. Fattal, "Single image dehazing," *ACM Trans. Graph.*, vol. 27, no. 3, pp. 1–9, 2008.

[12] K. He, J. Sun, and X. Tang, "Single image haze removal using dark channel prior," *IEEE Trans. Pattern Anal. Mach. Intell.*, vol. 33, no. 12, pp. 2341–2353, Dec. 2011.

[13] K. He, J. Sun, and X. Tang, "Guided image filtering," in *Proc. Eur. Conf. Comput. Vis.* Hong Kong: Springer, 2010, pp. 1–14.

[14] J. Pan, D. Sun, H. Pfister, and M.-H. Yang, "Blind image deblurring using dark channel prior," in *Proc. IEEE Conf. Comput. Vis. Pattern Recognit. (CVPR)*, Jun. 2016, pp. 1628–1636.

[15] S. Lee, S. Yun, J.-H. Nam, C. S. Won, and S.-W. Jung, "A review on dark channel prior based image dehazing algorithms," *EURASIP J. Image Video Process.*, vol. 2016, no. 1, pp. 1–23, Dec. 2016.

[16] Z. Fu, Y. Yang, C. Shu, Y. Li, H. Wu, and J. Xu, "Improved single image dehazing using dark channel prior," *J. Syst. Eng. Electron.*, vol. 26, no. 5, pp. 1070–1079, Oct. 2015.

[17] G. Obulesu, M. S. P. Kumar, P. Sowmya, and V. T. Reddy, "Single image dehazing using multilayer perceptron and DCP," *Int. J. Eng. Res.*, vol. 8, no. 3, pp. 205–209, 2019.

[18] G. Meng, Y. Wang, J. Duan, S. Xiang, and C. Pan, "Efficient image dehazing with boundary constraint and contextual regularization," in *Proc. IEEE Int. Conf. Comput. Vis.*, Dec. 2013, pp. 617–624.

[19] E. Koschmieder, "Bénard convection," *Adv. Chem. Phys*, vol. 26, pp. 177–212, Jan. 1974.

[20] J. Ahire, *Artificial Neural Networks: The Brain Behind Ai*. Morrisville, NC, USA: Lulu.com, 2018.

[21] Z.-H. Feng, J. Kittler, M. Awais, P. Huber, and X.-J. Wu, "Wing loss for robust facial landmark localisation with convolutional neural networks," in *Proc. IEEE/CVF Conf. Comput. Vis. Pattern Recognit.*, Jun. 2018, pp. 2235–2245.

[22] S. Chetlur, C. Woolley, P. Vandermersch, J. Cohen, J. Tran, B. Catanzaro, and E. Shelhamer, "CuDNN: Efficient primitives for deep learning," 2014, *arXiv:1410.0759*. [Online]. Available: http://arxiv.org/abs/1410.0759

[23] K. O'Shea and R. Nash, "An introduction to convolutional neural networks," 2015, *arXiv:1511.08458*. [Online]. Available: http://arxiv.org/abs/1511.08458

[24] V. Sharma and E. Elamaran, "Role of filter sizes in effective image classification using convolutional neural network," in *Cognitive Informatics and Soft Computing*. Mumbai, India: Springer, 2019, pp. 625–637.

[25] S. Albawi, T. A. Mohammed, and S. Al-Zawi, "Understanding of a convolutional neural network," in *Proc. Int. Conf. Eng. Technol. (ICET)*, Aug. 2017, pp. 1–6.

[26] R. Prabhu, *Understanding of Convolutional Neural Network (CNN)–Deep Learning*. San Francisco, CA, USA: A Medium Corporation, 2018.

[27] L. Cavigelli, D. Gschwend, C. Mayer, S. Willi, B. Muheim, and L. Benini, "Origami: A convolutional network accelerator," in *Proc. 25th Ed. Great Lakes Symp. VLSI*, 2015, pp. 199–204.

[28] C. Qu, D.-Y. Bi, P. Sui, A.-N. Chao, and Y.-F. Wang, "Robust dehaze algorithm for degraded image of CMOS image sensors," *Sensors*, vol. 17, no. 10, p. 2175, Sep. 2017.

[29] P. Cheng, S. He, J. Cheng, X. Luan, and F. Liu, "Asynchronous output feedback control for a class of conic-type nonlinear hidden Markov jump systems within a finite-time interval," *IEEE Trans. Syst., Man, Cybern. Syst.*, early access, Mar. 25, 2020, doi: 10.1109/TSMC.2020.2980312.

[30] P. Cheng, J. Wang, S. He, X. Luan, and F. Liu, "Observer-based asynchronous fault detection for conic-type nonlinear jumping systems and its application to separately excited DC motor," *IEEE Trans. Circuits Syst. I, Reg. Papers*, vol. 67, no. 3, pp. 951–962, Mar. 2020.

[31] P. Cheng, M. Chen, V. Stojanovic, and S. He, "Asynchronous fault detection filtering for piecewise homogenous Markov jump linear systems via a dual hidden Markov model," *Mech. Syst. Signal Process.*, vol. 151, Apr. 2021, Art. no. 107353.

[32] S. H. Park, S. Lee, I. D. Yun, and S. U. Lee, "Hierarchical MRF of globally consistent localized classifiers for 3D medical image segmentation," *Pattern Recognit.*, vol. 46, no. 9, pp. 2408–2419, Sep. 2013.

[33] L. R. Dice, "Measures of the amount of ecologic association between species," *Ecology*, vol. 26, no. 3, pp. 297–302, Jul. 1945.

[34] F. Monti, D. Boscaini, J. Masci, E. Rodola, J. Svoboda, and M. M. Bronstein, "Geometric deep learning on graphs and manifolds using mixture model CNNs," in *Proc. IEEE Conf. Comput. Vis. Pattern Recognit. (CVPR)*, Jul. 2017, pp. 5115–5124.

[35] M. Defferrard, X. Bresson, and P. Vandergheynst, "Convolutional neural networks on graphs with fast localized spectral filtering," in *Proc. Adv. Neural Inf. Process. Syst.*, 2016, pp. 3844–3852.

[36] L. Akoglu, H. Tong, and D. Koutra, "Graph based anomaly detection and description: A survey," *Data Mining Knowl. Discovery*, vol. 29, no. 3, pp. 626–688, May 2015.

[37] V. Garcia and J. Bruna, "Few-shot learning with graph neural networks," 2017, *arXiv:1711.04043*. [Online]. Available: http://arxiv.org/abs/1711.04043

[38] M. Narasimhan, S. Lazebnik, and A. Schwing, "Out of the box: Reasoning with graph convolution nets for factual visual question answering," in *Proc. Adv. Neural Inf. Process. Syst.*, 2018, pp. 2654–2665.

[39] Z. Cui, C. Xu, W. Zheng, and J. Yang, "Context-dependent diffusion network for visual relationship detection," in *Proc. 26th ACM Int. Conf. Multimedia*, Oct. 2018, pp. 1475–1482.

[40] D. Xu, Y. Zhu, C. B. Choy, and L. Fei-Fei, "Scene graph generation by iterative message passing," in *Proc. IEEE Conf. Comput. Vis. Pattern Recognit. (CVPR)*, Jul. 2017, pp. 5410–5419.

[41] B. Dai, Y. Zhang, and D. Lin, "Detecting visual relationships with deep relational networks," in *Proc. IEEE Conf. Comput. Vis. Pattern Recognit. (CVPR)*, Jul. 2017, pp. 3076–3086.

[42] J. Yang, J. Lu, S. Lee, D. Batra, and D. Parikh, "Graph R-CNN for scene graph generation," in *Proc. Eur. Conf. Comput. Vis. (ECCV)*, Sep. 2018, pp. 670–685.

[43] Q. Chen and V. Koltun, "Photographic image synthesis with cascaded refinement networks," in *Proc. IEEE Int. Conf. Comput. Vis. (ICCV)*, Oct. 2017, pp. 1511–1520.

[44] Y. Guo and A. S. Ashour, *Neutrosophic Set in Medical Image Analysis*. New York, NY, USA: Academic, 2019.

[45] M. Zhu and B. He, "Dehazing via graph cut," *Opt. Eng.*, vol. 56, no. 11, p. 1, Nov. 2017.

[46] C. Arora, S. Banerjee, P. Kalra, and S. Maheshwari, "An efficient graph cut algorithm for computer vision problems," in *Proc. Eur. Conf. Comput. Vis.* London, U.K.: Springer, 2010, pp. 552–565.

[47] P. Kohli and P. H. Torr, "Dynamic graph cuts and their applications in computer vision," in *Computer Vision*. London, U.K.: Springer, 2010, pp. 51–108.

[48] X. Liu, O. Veksler, and J. Samarabandu, "Order-preserving moves for Graph-Cut-Based optimization," *IEEE Trans. Pattern Anal. Mach. Intell.*, vol. 32, no. 7, pp. 1182–1196, Jul. 2010.

[49] L. Li, F. Wu, G. Yang, L. Xu, T. Wong, R. Mohiaddin, D. Firmin, J. Keegan, and X. Zhuang, "Atrial scar quantification via multi-scale CNN in the graph-cuts framework," *Med. Image Anal.*, vol. 60, Feb. 2020, Art. no. 101595.
[50] Y. Song, J. Li, X. Wang, and X. Chen, "Single image dehazing using ranking convolutional neural network," *IEEE Trans. Multimedia*, vol. 20, no. 6, pp. 1548–1560, Jun. 2018.
[51] C. E. Shannon, "A mathematical theory of communication," *Bell Syst. Tech. J.*, vol. 27, no. 3, pp. 379–423, Jul./Oct. 1948.
[52] R. M. Yousaf, H. A. Habib, Z. Mehmood, A. Banjar, R. Alharbey, and O. Aboulola, "Single image dehazing and edge preservation based on the dark channel probability-weighted moments," *Math. Problems Eng.*, vol. 2019, pp. 1–11, Dec. 2019.
[53] Y. Zhou, C. Shi, B. Lai, and G. Jimenez, "Contrast enhancement of medical images using a new version of the world cup optimization algorithm," *Quant. Imag. Med. Surg.*, vol. 9, no. 9, p. 1528, 2019.
[54] N. Hassan, S. Ullah, N. Bhatti, H. Mahmood, and M. Zia, "A cascaded approach for image defogging based on physical and enhancement models," *Signal, Image Video Process.*, vol. 14, pp. 867–875, Jan. 2020.

FAYADH S. ALENEZI (Member, IEEE) received the B.Sc. degree (Hons.) in electrical engineering electronics and communications track from Jouf University, Sakaka, Saudi Arabia, in 2012, the M.S. degree in electrical engineering from Southern Illinois University, Carbondale, IL, USA, in 2015, and the Ph.D. degree in electrical engineering from The University of Toledo, Toledo, OH, USA, in 2019. He is currently an Assistant Professor with the Department of Electrical Engineering, Jouf University. He has authored several journal and conference papers. His research interests include artificial intelligence, image processing, signal processing, image enchantment, machine learning, neural networks, and facial recognition.

SUBRAMANIAM GANESAN (Life Senior Member, IEEE) was the Chair of the Department of Computer Science and Engineering, from 1991 to 1998. He is currently a Professor with the Department of Electrical and Computer Engineering, Oakland University, Rochester, MI, USA. He has over 25 years of teaching and research experience in digital and automotive systems. He has published over 50 journal articles, 150 papers in conference proceedings, and three books. He has guided many Ph.D. theses as major advisor. He is a member of SAE, the IEEE Computer Society Distinguished Visiting Speaker, and a Council Member of ISPE. He is the Organizer for system engineering session at SAE World Congress for the past 15 years. He is the Editor-In-Chief of *International Journal of Embedded system and Computer Engineering*. His research interests include real-time systems, validation and verification, and modelling of computer systems for signal processing applications.